Network-Based Line-of-Sight Path Tracking of Underactuated Unmanned Surface Vehicles With Experiment Results

Wentao Wu, Zhouhua Peng, *Senior Member, IEEE*, Dan Wang, *Senior Member, IEEE*, Lu Liu, *Member, IEEE*, and Qing-Long Han, *Fellow, IEEE*

***Abstract*—This article deals with the problem of network-based path-tracking control of an underactuated unmanned surface vehicle subject to model uncertainties and unknown disturbances over a wireless network. A two-level network-based control architecture is proposed, including a local inner loop and a remote outer loop. In the remote outer loop, an event-triggered line-of-sight guidance law is designed to achieve path tracking while reducing the network burden for the remote control at the kinematic level. In the local inner loop, an extended state observer is employed to estimate the unknown disturbances due to the model uncertainties and environmental disturbances. Based on the estimated information from the extended state observer, an event-triggered anti-disturbance control law is developed to reduce the execution rate of actuators at the kinetic level. The stability of the closed-loop path-tracking system is proved based on the input-to-state stability and cascade stability theory. The effectiveness of the proposed network-based method for path tracking of the USV is verified via experiments.**

***Index Terms*—Event-trigger, extended state observer (ESO), line of sight (LOS), path tracking, unmanned surface vehicle (USV).**

Manuscript received May 2, 2020; revised November 20, 2020; accepted April 14, 2021. This work was supported in part by the National Natural Science Foundation of China under Grant 51979020, Grant 51909021, Grant 51939001, and Grant 52071044; in part by the Top-Notch Young Talents Program of China; in part by the Science and Technology Fund for Distinguished Young Scholars of Dalian under Grant 2018RJ08; in part by the Liaoning Revitalization Talents Program; in part by the Stable Supporting Fund of Science and Technology on Underwater Vehicle Technology under Grant JCKYS2019604SXJQR-01; in part by the Training Program for High-Level Technical Talent in Transportation Industry under Grant 2018-030; in part by the Fundamental Research Funds for the Central Universities under Grant 3132019319; and in part by the China Postdoctoral Science Foundation under Grant 2019M650086. This article was recommended by Associate Editor H.-B. Duan. *(Corresponding authors: Qing-Long Han; Zhouhua Peng.)*

Wentao Wu is with the School of Marine Electrical Engineering, Dalian Maritime University, Dalian 116026, China, and also with the Science and Technology on Underwater Vehicle Technology, Harbin Engineering University, Harbin 150001, China (e-mail: wuwentaodlmu@gmail.com).

Zhouhua Peng, Dan Wang, and Lu Liu are with the School of Marine Electrical Engineering, Dalian Maritime University, Dalian 116026, China (e-mail: zhpeng@dlmu.edu.cn; dwang@dlmu.edu.cn; wendaoerji@163.com).

Qing-Long Han is with the School of Software and Electrical Engineering, Swinburne University of Technology, Melbourne, VIC 3122, Australia (e-mail: qhan@swin.edu.au).

Color versions of one or more figures in this article are available at https://doi.org/10.1109/TCYB.2021.3074396.

Digital Object Identifier 10.1109/TCYB.2021.3074396

I. Introduction

In RECENT years, unmanned surface vehicles (USVs) have received considerable attention due to their ubiquitous advantages in several military and scientific applications [1], [2]. A variety of motion control scenarios is considered, such as trajectory tracking [3], [4]; target tracking [5]–[7]; path following [8]–[12]; target enclosing [13], [14]; and path tracking [15]–[17]. In order to achieve these motion scenarios, kinematic guidance law and kinetic control law are two critical components of any motion controllers. In the guidance loop, typical guidance methods includes line of sight (LOS) [18]–[20] and constant bearing guidance [21]. In the kinetic control loop, adaptive control [22], [23]; neural-network control [24], [25]; fuzzy control [21], [26]; sliding-mode control [27]; model predictive control [28], [29]; and extended-state-observer-based control [30]–[32] methods are widely used to account for model uncertainties and ocean disturbances. However, there are a few results which consider motion control of marine surface vehicles from a network standpoint.

With the fast development of unmanned and networked technologies, network-based control [33], [34] is the main trend for motion control of unmanned systems, including USVs. Some attempts have been made on motion control of USVs in network environments [26], [35]–[38]. In [26], a network-based fuzzy model is proposed for dynamic positioning of a USV subject to network-induced delays and packet dropouts. In [35], a network-based model is designed for a USV subject to actuator faults and external disturbances where network-induced delays and packet dropouts occurring in sampler-to-control station or control station-to-actuator channel are overcome. In [36], a network-based model is employed to stabilize the heading angle and reduce the rudder oscillations. In [37], a sampled-data design is presented in the synchronized path following where the path variables are updated in a discrete-time manner. In [38], an event-triggered modular-ISS neural-network control method is developed to reduce the communication burden during distributed formation control of multiple USVs. However, few works are available for network-based path tracking of USVs.

Motivated by the observations above, this article aims to address the network-based path-tracking control of a USV in

network environments. The USV suffers from model uncertainties and external ocean disturbances. A network-based control architecture is proposed for path tracking of the USV, which involves a local inner loop design and a remote outer loop design. Specifically, in the remote outer loop, an event-triggered guidance law based on the LOS principle is designed to achieve network-based path tracking without periodic communication. The network burden during the remote-control process can be decreased and the desired performance of path tracking still can be maintained under the constrained network. In the local inner loop, an extended state observer (ESO) is designed to estimate an unknown total disturbance composed of model uncertainties and environmental ocean disturbances. Based on the estimated disturbances from the ESO, an event-triggered anti-disturbance control law is developed to reduce the actuation burden at the kinetic level. Through input-to-state stability and cascade stability analysis, the stability of the closed-loop path-tracking system is proved, and all signals are uniformly ultimately bounded. Experiments are carried out to show the effectiveness of the proposed network-based method for path tracking of the USV.

The salient features of the proposed design method are as follows. First, compared with the results in [3]–[12], [17]–[20], and [16], [39], [40] without involving networks between the guidance loop and control loop, a network-based two-level control architecture is proposed for a USV which enables the separation of the guidance loop and the control loop in space. The advantage of the architecture is that the kinematic motion scenario can be achieved from the remote command center. Next, in contrast to the existing LOS guidance laws in [8]–[10], [19], [20], [30], and [41]–[43] based on the periodical sampling or communication, an event-triggered LOS guidance law is designed with aperiodic sampling or communication. Finally, in contrast to some kinetic control laws in [30], [31], and [45], based on the time-triggered ESOs, an event-triggered kinetic control law is designed herein based on the event-triggered ESOs, which can reduce the actuation and communication burden in the control loop. Besides, the proposed control law is much simpler than the event-triggered neural-network control law in [44], which facilitates practical implementations.

The organization of this article is arranged as follows. Section II presents the problem formulation. Section III gives the network-based control law design. Section IV presents the stability of the closed-loop path-tracking system. Section V provides experiment results for illustrations. Section VI concludes this article.

Notation: The following notations are used in this article. $\mathbb{N}^+$, $\mathbb{R}$, $\mathbb{R}^+$, and $\mathbb{R}^{n\times m}$ present a positive integer set, a real set, a positive real set, and an $n \times m$-dimensional matrix set, respectively. diag$\{\cdots\}$ and col$(\cdots)$, respectively, denote a block-diagonal matrix and a column vector. A^{T} describes the transpose of a matrix A. $|a|$ and $\|b\|$ present the absolute value of a real number a and the Euclidean norm of a vector b, respectively. $\lambda_{\max}(B)$ and $\lambda_{\min}(B)$ are the maximum eigenvalue and the minimum eigenvalue of a symmetric matrix B, respectively; I_n represents the identity matrix with n dimensions.

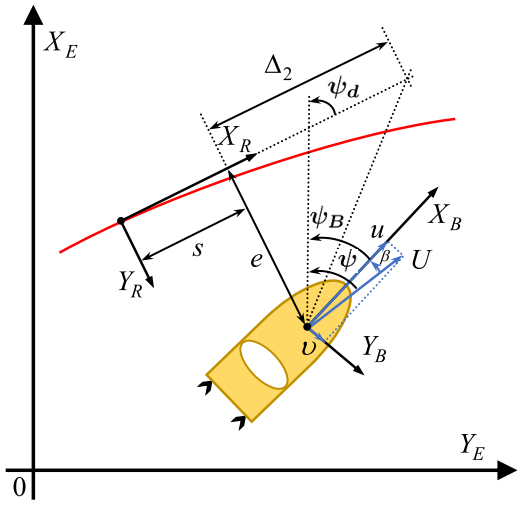

Fig. 1. LOS guidance.

II. Problem Formulation

As shown in Fig. 1, the mathematical model of a USV can be expressed in the north-east-down reference frame $X_E - Y_E$ and the body-fixed reference frame $X_B - Y_B$. The kinematic equation of the USV is expressed as [46]

$$\begin{cases} \dot{x} = U\cos\psi \\ \dot{y} = U\sin\psi \\ \dot{\psi} = r + \beta_d \end{cases} \tag{1}$$

where $x \in \mathbb{R}$ and $y \in \mathbb{R}$ are the position of the USV in $X_E - Y_E$; ψ presents its course angle in $X_E - Y_E$; $U = \sqrt{u^2 + v^2}$ is the total speed, where u and v denote the surge and sway speed expressed in $X_B - Y_B$, respectively; $r = \dot{\psi}_B$ denotes the angular velocity with ψ_B denoting the yaw angle; $\beta = \text{atan2}(v, u) \in (-\pi, \pi]$ is the sideslip angle in the reference frame $X_B - Y_B$, where atan2(v, u) is the four-quadrant version of arctan$(v/u) \in (-\pi/2, \pi/2)$; and $\beta_d = \dot{\beta}$ presents the time derivative of the sideslip angle.

The kinetic equation of the USV is described as [46]

$$\begin{cases} m_{11}\dot{u} = f_u(u, v, r) + \tau_u(t) + \tau_{uw}(t) \\ m_{22}\dot{v} = f_v(u, v, r) + \tau_{vw}(t) \\ m_{33}\dot{r} = f_r(u, v, r) + \tau_r(t) + \tau_{rw}(t) \end{cases} \tag{2}$$

where m_{11}, m_{22}, and m_{33} are the inertia of the USV; $f_u(u, v, r)$, $f_v(u, v, r)$, and $f_r(u, v, r)$ are the unknown functions, including Coriolis terms, damping terms, and unmodeled dynamics; τ_{uw}, τ_{vw}, and τ_{rw} are the unknown sea loads induced by wind, waves, and currents; and τ_u and τ_r are the control input torque and moment, respectively.

Note that $u = U\cos\beta$ and $v = U\sin\beta$. It follows from (2) that:

$$\begin{cases} m_{11}\dot{U} = \cos\beta(f_u(u, v, r) + \tau_{uw}) \\ \qquad + \sin\beta(\tau_{vw} + f_v(u, v, r))\dfrac{m_{11}}{m_{22}} - 2\tau_u\sin^2\left(\dfrac{\beta}{2}\right) \\ \qquad - m_{11}\beta_d(v\cos\beta + u\sin\beta) + \tau_u \\ m_{33}\dot{r} = f_r(u, v, r) + \tau_{rw} + \tau_r. \end{cases} \tag{3}$$

Consider a path expressed as $p_d = \text{col}(x_d(\theta), y_d(\theta)) \in \mathbb{R}^2$, where $\theta \in \mathbb{R}$ is a path variable. Define two kinematic tracking errors as

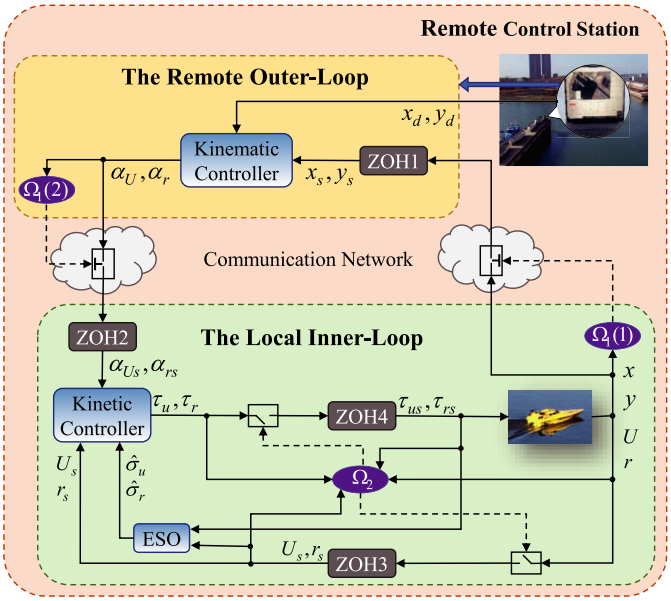

Fig. 2. Two-level network-based guidance and control architecture.

$$\begin{bmatrix} s \\ e \end{bmatrix} = \begin{bmatrix} \cos(\psi_d) & -\sin(\psi_d) \\ \sin(\psi_d) & \cos(\psi_d) \end{bmatrix}^{\mathrm{T}} \begin{bmatrix} x - x_d(\theta) \\ y - y_d(\theta) \end{bmatrix} \tag{4}$$

where s and e are the along-track error and cross-track error; $\psi_d = \text{atan2}(\dot{y}_d(\theta), \dot{x}_d(\theta))$ denotes the path-tangential angle with $\dot{y}_d(\theta) = \partial y_d(\theta)/\partial\theta$ and $\dot{x}_d(\theta) = \partial x_d(\theta)/\partial\theta$. The following assumption is needed in this article.

Assumption 1: The signals of the parameterized path $p_d(\theta)$ $\partial p_d(\theta)/\partial\theta$ and $\partial^2 p_d(\theta)/\partial^2\theta$ are bounded.

The control objective of this article is to develop a network-based path-tracking control law for the USV described by (1) and (2) such that

$$\lim_{t\to\infty} |s| \le l_s^*, \lim_{t\to\infty} |e| \le l_e^* \tag{5}$$

where l_s^* and l_e^* are positive constants.

III. Design and Analysis

In this section, an event-triggered two-level network-based control architecture is presented. This architecture includes a local inner loop design and a remote outer loop design shown in Fig. 2.

A. Remote Outer Loop Guidance Law

In this section, a remote outer loop guidance law is first proposed based on an LOS guidance scheme and an event-triggered scheme. Then, some triggering conditions are presented for scheduling the data transmissions. Finally, the input-to-state stability of the guidance loop is analyzed.

1) Guidance Law Design: Taking the time derivative of (4) and using (1), it follows that:

$$\begin{cases} \dot{s} = U\cos(\psi - \psi_d) + er_d - u_0 U_d \\ \dot{e} = U\sin(\psi - \psi_d) - sr_d \\ \dot{\psi} = r + \beta_d \end{cases} \tag{6}$$

where $U_d = \sqrt{\dot{x}_d^2(\theta) + \dot{y}_d^2(\theta)}$, $r_d = \dot{\psi}_d$, and $\dot{\theta} = u_0$ with $(u_0 \in \mathbb{R}^+)$ being a given update velocity of the path variable.

Define $\epsilon_U = \alpha_{Us} - \alpha_U$, $q_U = U - \alpha_{Us}$, $\epsilon_r = \alpha_{rs} - \alpha_r$, $q_r = r - \alpha_{rs}$, and $\psi_e = \psi - \alpha_\psi$, where α_U, α_r, and α_ψ are the desired guidance signals; and α_{Us} and α_{rs} denote the sampling signals stored in the zero order holder (ZOH). The signal is maintained as a constant in the ZOH for the whole sampling period. The sampling signal stored in the ZOH will be updated until the corresponding event-triggered condition is satisfied. For a sampling period $t \in [t_i^\eta, t_{i+1}^\eta)$ from the ith to the $(i+1)$th releasing state of the USV over the wireless network, the kinematic tracking error dynamics in (6) can be written as

$$\begin{cases} \dot{s} = \alpha_U + \epsilon_U + q_U + er_d - u_0 U_d \\ \qquad - 2U\sin^2\left(\dfrac{\psi - \psi_d}{2}\right) \\ \dot{e} = U\sin\left(\alpha_\psi - \psi_d\right) + \varepsilon - sr_d \\ \dot{\psi}_e = \alpha_r + \epsilon_r + q_r + \beta_d - \dot{\alpha}_\psi \end{cases} \tag{7}$$

where $\varepsilon = 2U\sin(\psi_e/2)\cos((\psi + \alpha_\psi - 2\psi_d)/2)$. Based on (4), the sampling path tracking errors s_s and e_s are defined as

$$\begin{bmatrix} s_s \\ e_s \end{bmatrix} = \begin{bmatrix} \cos(\psi_d) & -\sin(\psi_d) \\ \sin(\psi_d) & \cos(\psi_d) \end{bmatrix}^{\mathrm{T}} \begin{bmatrix} x_s - x_d(\theta) \\ y_s - y_d(\theta) \end{bmatrix}. \tag{8}$$

To stabilize (7), an event-triggered LOS guidance law is proposed as

$$\begin{cases} \alpha_U = -\dfrac{k_1 s_s}{\sqrt{s_s^2 + \Delta_1^2}} + u_0 U_d \\ \alpha_\psi = -\arctan\left(\dfrac{e_s}{\Delta_2}\right) + \psi_d \\ \alpha_r = -\dfrac{k_2 \psi_e}{\sqrt{\psi_e^2 + \Delta_3^2}} + r_d \end{cases} \tag{9}$$

where $k_1, k_2 \in \mathbb{R}^+$ are control gains; $\Delta_1, \Delta_3 \in \mathbb{R}^+$ are constants; $\Delta_2 \in \mathbb{R}^+$ is a look-ahead distance.

Substituting (9) into (7), the dynamics of the kinematic tracking errors are written as

$$\begin{cases} \dot{s} = -\underline{k}_1(s + \epsilon_s) + \epsilon_U + q_U + er_d \\ \qquad - 2U\sin^2\left(\dfrac{\psi - \psi_d}{2}\right) \\ \dot{e} = -\underline{k}_2(e + \epsilon_e) + \varepsilon - sr_d \\ \dot{\psi}_e = -\underline{k}_3\psi_e + \epsilon_r + q_r + \beta_d \end{cases} \tag{10}$$

where $\underline{k}_1 = k_1/\sqrt{s_s^2 + \Delta_1^2}$, $\underline{k}_2 = U/\sqrt{e_s^2 + \Delta_2^2}$, and $\underline{k}_3 = k_2/\sqrt{\psi_e^2 + \Delta_3^2}$ which can be considered as time-varying gains; $\epsilon_s = s_s - s$ and $\epsilon_e = e_s - e$ are errors between the triggered path tracking errors and practical path tracking errors.

2) Kinematic Event-Triggered Data Transmission: As shown in Fig. 2, there are two network channels between the remote outer loop and the local inner loop. To reduce the communication burden, the triggering conditions Ω_1 are described as

$$\begin{cases} \Omega_1(1) : \|\eta_s(t) - \eta(t)\| \le \epsilon_\eta^* \\ \Omega_1(2) : \|\alpha_s(t) - \alpha(t)\| \le \epsilon_\alpha^* \end{cases} \tag{11}$$

where $\eta(t) = \text{col}(x(t), y(t), \psi(t))$ and $\alpha(t) = \text{col}(\alpha_U(t), \alpha_r(t))$; $\eta_s(t)$ and $\alpha_s(t)$ present the sampling signals stored in ZOH1. $\epsilon_\eta^* \in \mathbb{R}^+$ and $\epsilon_\alpha^* \in \mathbb{R}^+$ are the predefined triggering thresholds.

To be more specific, the variable $t_i^\eta \in \mathbb{R}^+$ with $i \in \mathbb{N}^+$ denotes the ith triggering time with the initial time t_0^η. The event detector in the local loop continuously compares the tacking errors by the $\Omega_1(1)$. If $\Omega_1(1)$ is false at t_{i+1}^η, the state information at t_{i+1}^η is transmitted to store the ZOH1 over the wireless network. During $[t_i^\eta, t_{i+1}^\eta)$, the wireless network associated with the ZOH2 can be triggered to transmit the desired commands for the USV only if $\Omega_1(2)$ is not satisfied. Similarly, let $t_j^\alpha \in \mathbb{R}^+$ with $j \in \mathbb{N}^+$ present the releasing moment of the desired signals.

3) Stability Analysis: We first analyze the stability of the event-triggered kinematic subsystem (10).

Lemma 1: Under Assumption 1, the event-triggered kinematic subsystem (10): $[z_e, \alpha_e, q, U, \beta_d] \mapsto z_1$ is input-to-state stable (ISS).

Proof: Consider a Lyapunov function as

$$V_1 = \frac{1}{2}\left(s^2 + e^2 + \psi_e^2\right). \tag{12}$$

Taking the time derivative of V_1 for $t \in [t_i^\eta, t_{i+1}^\eta)$ along (10) yields

$$\begin{aligned} \dot{V}_1 = &-\underline{k}_1 s^2 - \underline{k}_2 e^2 - \underline{k}_3 \psi_e^2 - \underline{k}_1 s\epsilon_s - \underline{k}_2 e\epsilon_e \\ &+ s\epsilon_U + \psi_e \epsilon_r + sq_U + \psi_e q_r + e\varepsilon + \psi_e \beta_d \\ &- 2sU\sin^2\left(\frac{\psi - \psi_d}{2}\right). \end{aligned} \tag{13}$$

Let $z_1 = \text{col}(s, e, \psi_e)$. Rewrite (13) as

$$\begin{aligned} \dot{V}_1 \le -c_1\|z_1\|^2 + \|z_1\|(&\lambda_{\max}(K)\|z_e\| + \|\alpha_e\| \\ &+ \|q\| + |\beta_d| + 2|U|) \end{aligned} \tag{14}$$

where $K = \text{diag}\{\underline{k}_1, \underline{k}_2, \underline{k}_3\}$, $c_1 = \lambda_{\min}(K)$, $z_e = \text{col}(\epsilon_s, \epsilon_e)$, $\alpha_e = \text{col}(\epsilon_U, \epsilon_r)$, and $q = \text{col}(q_U, q_r)$.

As

$$\|z_1\| \ge \frac{\lambda_{\max}(K)\|z_e\| + \|\alpha_e\| + \|q\| + |\beta_d| + 2|U|}{c_1\kappa_1} \tag{15}$$

it renders that

$$\dot{V}_1 \le -c_1(1 - \kappa_1)\|z_1\|^2 \tag{16}$$

where $0 < \kappa_1 < 1$.

Thus, it is concluded that the even-triggered kinematic subsystem (10) is ISS [47], and the ultimate bound is given by

$$\begin{aligned} \|z_1\| \le \max\Bigg\{&\|z_1(t_0)\|e^{-c_1(1-\kappa_1)(t-t_0)}, \frac{\|\alpha_e\|}{c_1\kappa_1} \\ &+ \frac{\lambda_{\max}(K)\|z_e\| + \|q\| + |\beta_d| + 2|U|}{c_1\kappa_1}\Bigg\}. \end{aligned} \tag{17}$$

The proof is completed. ■

B. Local Inner Loop Control Law

In this section, an event-triggered kinetic control law is first developed by using the estimated information from ESOs. Then, the event-triggering conditions are presented for the inner loop such that the actuation times can be reduced. Finally, the stability of the inner loop is analyzed.

1) Event-Triggered Control Law Design: To facilitate the ESO design, rewrite (3) as

$$\begin{cases} \dot{U} = \sigma_u(u, v, r, t) + \dfrac{\tau_u}{m_{11}} \\ \dot{r} = \sigma_r(u, v, r, t) + \dfrac{\tau_r}{m_{33}} \end{cases} \tag{18}$$

where $\sigma_u(u, v, r, t) = \cos\beta(f_u(u, v, r) + \tau_{uw})/m_{11} + \sin\beta(f_v(u, v, r) + \tau_{vw})/m_{22} - \beta_d(v\cos\beta + u\sin\beta) - 2\tau_u\sin^2(\beta/2)/m_{11}$ and $\sigma_r(u, v, r, t) = (f_r(u, v, r) + \tau_{rw})/m_{33}$.

Let $\hat{U}$, $\hat{\sigma}_u$, $\hat{r}$, and $\hat{\sigma}_r$ be the estimates of U, σ_u, r, and σ_r, respectively. Two ESOs based on the triggered signals U_s and r_s are used to estimate σ_u and σ_r as

$$\begin{cases} \dot{\hat{U}} = -k_1^u\left(\hat{U} - U_s\right) + \hat{\sigma}_u + \dfrac{\tau_{us}}{m_{11}} \\ \dot{\hat{\sigma}}_u = -k_2^u\left(\hat{U} - U_s\right) \\ \dot{\hat{r}} = -k_1^r\left(\hat{r} - r_s\right) + \hat{\sigma}_r + \dfrac{\tau_{rs}}{m_{33}} \\ \dot{\hat{\sigma}}_r = -k_2^r\left(\hat{r} - r_s\right) \end{cases} \tag{19}$$

where k_1^u, k_2^u, k_1^r, and $k_2^r \in \mathbb{R}^+$ are observer parameters. Define the estimation errors $\vartheta_U = \hat{U} - \alpha_{Us}$ and $\vartheta_r = \hat{r} - \alpha_{rs}$. Taking the time derivative of ϑ_U and ϑ_r over a control interval $t \in [t_m^\tau, t_{m+1}^\tau)$, respectively, we have

$$\begin{cases} \dot{\vartheta}_U = -k_1^u\left(\tilde{U} - U_e\right) + \hat{\sigma}_u + \dfrac{\tau_{us}}{m_{11}} \\ \dot{\vartheta}_r = -k_1^r(\tilde{r} - r_e) + \hat{\sigma}_r + \dfrac{\tau_{rs}}{m_{33}} \end{cases} \tag{20}$$

where $\tilde{U} = \hat{U} - U$ and $\tilde{r} = \hat{r} - r$.

An anti-disturbance kinetic control law is designed to stabilize the dynamics of ϑ_U and ϑ_r as

$$\begin{cases} \tau_u = m_{11}\left(-k_u(U_s - \alpha_{Us}) - \hat{\sigma}_u\right) \\ \tau_r = m_{33}\left(-k_r(r_s - \alpha_{rs}) - \hat{\sigma}_r\right) \end{cases} \tag{21}$$

where $k_u \in \mathbb{R}^+$ and $k_r \in \mathbb{R}^+$ are control gains.

Let $\tau_{ue} = \tau_{us} - \tau_u$ and $\tau_{re} = \tau_{rs} - \tau_r$, Substituting (21) into (20), we have the time derivative of ϑ_U and ϑ_r as

$$\begin{cases} \dot{\vartheta}_U = -k_u\vartheta_U - k_e^u\big(\tilde{U} - U_e\big) + \dfrac{\tau_{ue}}{m_{11}} \\ \dot{\vartheta}_r = -k_r\vartheta_r - k_e^r(\tilde{r} - r_e) + \dfrac{\tau_{re}}{m_{33}} \end{cases} \tag{22}$$

where $k_e^u = k_1^u - k_u$ and $k_e^r = k_1^r - k_r$.

Define $\tilde{\sigma}_u = \hat{\sigma}_u - \sigma_u$ and $\tilde{\sigma}_r = \hat{\sigma}_r - \sigma_r$. To make it easier to analyze the stability of the kinetic subsystem, the error dynamics of the (19) can be expressed as

$$\begin{cases} \dot{\tilde{U}} = -k_1^u\tilde{U} + \tilde{\sigma}_u + k_1^u U_e + \dfrac{\tau_{ue}}{m_{11}} \\ \dot{\tilde{\sigma}}_u = -k_2^u\tilde{U} + k_2^u U_e - \dot{\sigma}_u \\ \dot{\tilde{r}} = -k_1^r\tilde{r} + \tilde{\sigma}_r + k_1^r r_e + \dfrac{\tau_{re}}{m_{33}} \\ \dot{\tilde{\sigma}}_r = -k_2^r\tilde{r} + k_2^r r_e - \dot{\sigma}_r. \end{cases} \tag{23}$$

Let $z_2 = \mathrm{col}(\tilde{U}, \tilde{\sigma}_u, \tilde{r}, \tilde{\sigma}_r)$. It follows from (23) that:

$$\dot{z}_2 = A_1 z_2 + B_1\nu_e + B_2\tau_e - B_3\dot{\sigma} \tag{24}$$

where $\nu_e = \nu_s(t) - \nu(t) = \mathrm{col}(U_e, r_e)$, $\tau_e = \tau_s(t) - \tau(t) = \mathrm{col}(\tau_{ue}, \tau_{re})$, $\dot{\sigma} = \mathrm{col}(\dot{\sigma}_u, \dot{\sigma}_r)$, and

$$\begin{cases} A_1 = \begin{bmatrix} -k_1^u & 1 & 0 & 0 \\ -k_2^u & 0 & 0 & 0 \\ 0 & 0 & -k_1^r & 1 \\ 0 & 0 & -k_2^r & 0 \end{bmatrix} \\ B_1 = \begin{bmatrix} k_1^u & k_2^u & 0 & 0 \\ 0 & 0 & k_1^r & k_2^r \end{bmatrix}^{\mathrm{T}} \\ B_2 = \begin{bmatrix} \frac{1}{m_{11}} & 0 & 0 & 0 \\ 0 & 0 & \frac{1}{m_{33}} & 0 \end{bmatrix}^{\mathrm{T}} \\ B_3 = \begin{bmatrix} 0 & 1 & 0 & 0 \\ 0 & 0 & 0 & 1 \end{bmatrix}^{\mathrm{T}}. \end{cases} \tag{25}$$

Note that the matrix A_1 is a Hurwitz matrix. There exists a positive-definite matrix P_1 satisfying the following inequality:

$$A_1^{\mathrm{T}}P_1 + P_1A_1 \le -c_2 I_1 \tag{26}$$

where $c_2 \in \mathbb{R}^+$.

2) Kinetic Event-Triggered Data Transmission: As shown in Fig. 2, an event-triggered condition Ω_2 is presented to determine the event-triggered schedule to transmit the data. Two triggering thresholds are given as

$$\begin{cases} \Omega_2(1) : \|\nu_s(t) - \nu(t)\| \le \epsilon_\nu^* \\ \Omega_2(2) : \|\tau_s(t) - \tau(t)\| \le \epsilon_\tau^* \\ \Omega_2(3) : \nu_s \text{ is transmitted into the controller (21)} \end{cases} \tag{27}$$

where $\nu(t) = \mathrm{col}(U(t), r(t))$, and $\tau(t) = \mathrm{col}(\tau_u(t), \tau_r(t))$, $\nu_s(t)$ and $\tau_s(t)$ denote the sampling signal, $\epsilon_\nu^* \in \mathbb{R}^+$ and $\epsilon_\tau^* \in \mathbb{R}^+$ are the triggering thresholds.

In the local loop, define the data transmission moment $t_m^\nu \in \mathbb{R}^+$ with $m \in \mathbb{N}^+$ from the actuator to controller. Under $\Omega_2(1)$ false condition, the previous data $\nu(t_m^\nu)$ stored in the ZOH3 is updated at t_{m+1}^ν. The estimator (19) and controller (21) will recalculate the estimated disturbances and control inputs of the USV using data updated in ZOH3. If the triggering condition $\Omega_2(2)$ is not satisfied, the control inputs in the ZOH4 will be updated over $[t_m^\nu, t_{m+1}^\nu)$. Let $t_n^\tau \in \mathbb{R}^+$ with $n \in \mathbb{N}^+$ represent the triggering time if $\Omega_2(2)$ is false.

3) Stability Analysis: We now analyze the stability of the kinetic subsystem (22) and the ESO subsystem (24). The following assumption is needed.

Assumption 2: The time derivatives of $\sigma_u(\cdot)$ and $\sigma_r(\cdot)$ are bounded and satisfy $|\dot{\sigma}_u| \le \dot{\sigma}_u^*$ with $\dot{\sigma}_u^* \in \mathbb{R}^+$ and $|\dot{\sigma}_r| \le \dot{\sigma}_r^*$ with $\dot{\sigma}_r^* \in \mathbb{R}^+$.

Lemma 2: Under Assumption 2, the ESO subsystem (24): $[\nu_e, \tau_e, \dot{\sigma}] \mapsto [z_2]$ is ISS.

Proof: Construct a Lyapunov function as

$$V_2 = \frac{1}{2}z_2^{\mathrm{T}}P_1 z_2. \tag{28}$$

Taking the time derivative of V_2 along (24) over $[t_n^\tau, t_{n+1}^\tau)$, it follows that:

$$\dot{V}_2 = z_2^{\mathrm{T}}P_1(A_1 z_2 + B_1\nu_e + B_2\tau_e - B_3\dot{\sigma}). \tag{29}$$

Using (26), it follows that:

$$\begin{aligned} \dot{V}_2 \le -\frac{c_2\|z_2\|^2}{2} + \|z_2\|(\|P_1B_1\|\|\nu_e\| + \|P_1B_2\|\|\tau_e\| \\ + \|P_1B_3\|\|\dot{\sigma}\|) \end{aligned} \tag{30}$$

where $0 < \kappa_2 < 1$.

As

$$\|z_2\| \ge \frac{2(\|P_1B_1\|\|\nu_e\| + \|P_1B_2\|\|\tau_e\|)}{c_2\kappa_2} + \frac{2\|P_1B_3\|\|\dot{\sigma}\|}{c_2\kappa_2} \tag{31}$$

under (30), it follows that:

$$\dot{V}_2 \le -\frac{c_2}{2}(1 - \kappa_2)\|z_2\|^2. \tag{32}$$

Therefore, the ESO subsystem (24) is ISS and the ultimate bound is given by

$$\begin{aligned} \|z_2\| \le \max\Bigg\{ & \|z_2(t_0)\|e^{-\frac{c_2(1-\kappa_2)(t-t_0)}{2}}, 2\sqrt{\lambda_{\max}(P_1)} \\ & \times \frac{\|P_1B_1\|\|\nu_e\| + \|P_1B_2\|\|\tau_e\| + \|P_1B_3\|\|\dot{\sigma}\|}{c_2\kappa_2\sqrt{\lambda_{\min}(P_1)}} \Bigg\}. \end{aligned} \tag{33}$$

The proof is completed. ■

Lemma 3: The kinetic subsystem (22): $[\tilde{U}, \tilde{r}, \nu_e, \tau_e] \mapsto [z_3]$ is ISS.

Proof: Define a Lyapunov function as

$$V_3 = \frac{1}{2}\Big(\vartheta_U^2 + \vartheta_r^2\Big). \tag{34}$$

Taking the time derivative of V_3 and using (22) over $[t_m^\nu, t_{m+1}^\nu)$, it renders

$$\begin{aligned} \dot{V}_3 = & -k_u\vartheta_U^2 - k_r\vartheta_r^2 - k_e^u\tilde{U}\vartheta_U - k_e^r\tilde{r}\vartheta_r + k_e^u U_e\vartheta_U \\ & + k_e^r r_e\vartheta_r + \frac{\tau_{ue}}{m_{11}}\vartheta_U + \frac{\tau_{re}}{m_{33}}\vartheta_r. \end{aligned} \tag{35}$$

Noting that $z_3 = \mathrm{col}(\vartheta_U, \vartheta_r)$ and $c_3 = \lambda_{\min}\{k_u, k_r\}$, one has

$$\begin{aligned} \dot{V}_3 \le & -c_3\|z_3\|^2 + \big(k_e^u + k_e^r\big)\|z_2\|\|z_3\| \\ & + \big(\lambda_{\max}\big(K_e^\nu\big)\|\nu_e\| + \lambda_{\max}(K_m)\|\tau_e\|\big)\|z_3\| \end{aligned} \tag{36}$$

where $K_e^v = \text{diag}\{k_e^u, k_e^r\}$ and $K_m = \text{diag}\{1/m_{11}, 1/m_{33}\}$.

Since

$$\|z_3\| \geq \frac{\left(k_e^u + k_e^r\right)\|z_2\| + \lambda_{\max}\left(K_e^v\right)\|v_e\|}{\kappa_3 c_3} + \frac{\lambda_{\max}(K_m)\|\tau_e\|}{\kappa_3 c_3} \tag{37}$$

it follows that:

$$\dot{z}_3 \leq -c_3(1-\kappa_3)\|z_3\|^2 \tag{38}$$

where $0 < \kappa_3 < 1$.

Therefore, one can conclude that the kinetic subsystem (22) is ISS by [47], and the ultimate bound is given by

$$\|z_3\| \leq \max\left\{\|z_3(t_0)\|e^{-\frac{c_3(1-\kappa_3)(t-t_0)}{2}}, \frac{k_e^u + k_e^r}{\kappa_3 c_3}\|z_2\| + \frac{\lambda_{\max}\left(K_e^v\right)\|v_e\| + \lambda_{\max}(K_m)\|\tau_e\|}{\kappa_3 c_3}\right\}. \tag{39}$$

The proof is completed. ■

IV. Stability Analysis

In the previous section, the stability of the subsystems (10), (22), and (24) are analyzed. In this section, the stability of the cascade system consisted of kinematic guidance subsystem (10) and kinetic control subsystem (22) is stated in the following theorem.

Theorem 1: Consider the underactuated USV described by (1) and (2), the event-triggered network-based path-tracking guidance law in (9), the ESOs in (19), the kinetic control law in (22), and the event-triggered conditions in (11) and (27). Under Assumptions 1 and 2, the closed-loop system is ISS and all error signals in the closed-loop network system are bounded.

Proof: Note that

$$\begin{cases} q_U = \vartheta_U - \tilde{U} \leq |\vartheta_U| + \left|\tilde{U}\right| \\ q_r = \vartheta_r - \tilde{r} \leq |\vartheta_r| + |\tilde{r}|. \end{cases} \tag{40}$$

We have

$$q = z_3 - \tilde{\nu} \leq \|z_3\| + \|\tilde{\nu}\| \leq \|z_2\| + \|z_3\|. \tag{41}$$

Note also that

$$\begin{aligned} U &= q_U + \alpha_U + \epsilon_U \\ &\leq |\vartheta_U| + \left|\tilde{U}\right| + |\alpha_U| + |\epsilon_U| \\ &\leq \|z_2\| + \|z_3\| + |\alpha_U| + |\epsilon_U|. \end{aligned} \tag{42}$$

We have

$$\|z_1\| \leq \max\left\{\|z_1(t_0)\|e^{-c_1(1-\kappa_1)(t-t_0)}, \frac{\|\alpha_e\| + |\beta_d|}{c_1\kappa_1} + \frac{\lambda_{\max}(K)\|z_e\| + |\alpha_U| + |\epsilon_U| + 3(\|z_2\| + \|z_3\|)}{c_1\kappa_1}\right\}. \tag{43}$$

According to [47] and Lemmas 1–3, the closed-loop system is ISS. As $t \to \infty$, it follows that:

$$\begin{cases} \|z_1\| \leq 6\left(\|P_1B_1\|\epsilon_v^* + \|P_1B_2\|\epsilon_\tau^* + \|P_1B_3\|\dot{\sigma}^*\right) \times \frac{\left(k_e^u + k_e^r + c_3\kappa_3\right)\sqrt{\lambda_{\max}(P_1)}}{c_1c_2c_3\kappa_1\kappa_2\kappa_3\sqrt{\lambda_{\min}(P_1)}} + \frac{3\left(\lambda_{\max}\left(K_e^v\right)\epsilon_v^* + \lambda_{\max}(K_m)\epsilon_\tau^*\right)}{c_1c_3\kappa_1\kappa_3} + \frac{\lambda_{\max}(K)\epsilon_z^* + 2\epsilon_\alpha^* + k_1 + u_0U_d^* + \beta_d^*}{c_1\kappa_1} \\ \|z_2\| \leq \frac{2\left(\|P_1B_1\|\epsilon_v^* + \|P_1B_2\|\epsilon_\tau^*\right)\sqrt{\lambda_{\max}(P_1)}}{c_2\kappa_2\sqrt{\lambda_{\min}(P_1)}} + \frac{2\|P_1B_3\|\sigma^*\sqrt{\lambda_{\max}(P_1)}}{c_2\kappa_2\sqrt{\lambda_{\min}(P_1)}} \\ \|z_3\| \leq 2\left(\|P_1B_1\|\epsilon_v^* + \|P_1B_2\|\epsilon_\tau^* + \|P_1B_3\|\dot{\sigma}^*\right) \times \frac{\left(k_e^u + k_e^r\right)\sqrt{\lambda_{\max}(P_1)}}{c_2c_3\kappa_2\kappa_3\sqrt{\lambda_{\min}(P_1)}} + \frac{\lambda_{\max}\left(K_e^v\right)}{c_3\kappa_3}\epsilon_v^* + \frac{\lambda_{\max}(K_m)}{c_3\kappa_3}\epsilon_\tau^*. \end{cases} \tag{44}$$

■

As a result, all error signals in the cascade system are uniformly ultimately bounded.

Remark 1: It is worth noting that the sampling virtual guidance law $\dot{\alpha}_s = 0$ over the period $[t_j^\alpha, t_{j+1}^\alpha)$ such that the repeated differentiation of the virtual control law is not required. ZOHs are used to hold the sampling data and thus there is a jump on the sampling moment t_s. The difference of the sampled data on t_s^- and t_s^+ is a bounded measurement such that the jump bounce exists. As a result, the jump produced by the ZOHs can be considered as a bounded perturbation.

Remark 2: By Theorem 1, the tracking performance of the closed-loop system relates to the event-triggered thresholds. Upper bounds of these errors are determined by the corresponding triggered thresholds. Hence, there is a trade-off between the desired performance and the triggering thresholds.

Theorem 2: Under the event-triggered mechanism (11) and (27), there exist positive constants ϱ_η, ϱ_α, ϱ_ν, and ϱ_τ such that the communication intervals $t_{i+1}^\eta - t_i^\eta \geq \varrho_\eta$, $t_{j+1}^\alpha - t_j^\alpha \geq \varrho_\alpha$, $t_{m+1}^\nu - t_m^\nu \geq \varrho_\nu$, and $t_{n+1}^\tau - t_n^\tau \geq \varrho_\tau$, and Zeno behaviors are excluded.

Proof: The time derivation of the triggering condition $\Omega_1(1)$ with $t \in [t_i^\eta, t_{i+1}^\eta)$, $\Omega_1(2)$ with $t \in [t_j^\alpha, t_{j+1}^\alpha)$, $\Omega_2(1)$ with $t \in$

$[t_m^v, t_{m+1}^v)$ and $\Omega_2(2)$ with $t \in [t_n^\tau, t_{n+1}^\tau)$ are as follows:

$$\begin{cases} \|\dot{\eta}_e\| = \|\dot{\eta}_s(t) - \dot{\eta}(t)\| \\ \quad \le \|\mathrm{col}(U\cos\psi, U\sin\psi, r + \beta_d)\| \\ \|\dot{\alpha}_e\| = \|\dot{\alpha}_s(t) - \dot{\alpha}(t)\| \\ \quad \le \left\|\mathrm{col}\left(u_0\dot{U}_d, |\underline{k}_3\dot{\psi}_e|\left(\Delta_3^2 - \psi_e^2\right) + \dot{r}_d\right)\right\| \\ \|\dot{\nu}_e\| = \|\dot{\nu}_s(t) - \dot{\nu}(t)\| \\ \quad \le \|\sigma\| + \lambda_{\max}(K_m)\|\tau\| \\ \|\dot{\tau}_e\| = \|\dot{\tau}_s(t) - \dot{\tau}(t)\| \\ \quad \le \lambda_{\max}(K_m)\left|\dot{\hat{\sigma}}\right|. \end{cases} \tag{45}$$

Under Assumptions 1, 2, and by Theorem 1, U, $\dot{U}_d$, r, $\dot{r}_d$, β_d, ψ_e, σ, τ, and $\hat{\sigma}$ are bounded. Therefore, $\dot{\eta}_e$, $\dot{\alpha}_e$, $\dot{\nu}_e$, and $\dot{\tau}_e$ all have upper bounds denoting $\hbar_\eta$, $\hbar_\alpha$, $\hbar_\nu$, and $\hbar_\tau$, respectively. The initial conditions are satisfied as follows:

$$\begin{cases} \lim_{t\to t_i^{\eta+}} \|\eta_s(t) - \eta(t)\| = 0 \\ \lim_{t\to t_j^{\alpha+}} \|\alpha_s(t) - \alpha(t)\| = 0 \\ \lim_{t\to t_m^{\nu+}} \|\nu_s(t) - \nu(t)\| = 0 \\ \lim_{t\to t_n^{\tau+}} \|\tau_s(t) - \tau(t)\| = 0. \end{cases} \tag{46}$$

The errors can be rendered as

$$\begin{cases} \|\eta_s(t) - \eta(t)\| \le \hbar_\eta\left(t - t_i^\eta\right), & t \in \left[t_i^\eta, t_{i+1}^\eta\right) \\ \|\alpha_s(t) - \alpha(t)\| \le \hbar_\alpha\left(t - t_j^\alpha\right), & t \in \left[t_j^\alpha, t_{j+1}^\alpha\right) \\ \|\nu_s(t) - \nu(t)\| \le \hbar_\nu\left(t - t_m^\nu\right), & t \in \left[t_m^\nu, t_{m+1}^\nu\right) \\ \|\tau_s(t) - \tau(t)\| \le \hbar_\tau\left(t - t_n^\tau\right), & t \in \left[t_n^\tau, t_{n+1}^\tau\right). \end{cases} \tag{47}$$

When the triggering conditions $\Omega_1(1)$, $\Omega_1(2)$, $\Omega_2(1)$, and $\Omega_2(2)$ are not satisfied, we have

$$\begin{cases} \lim_{t\to t_{i+1}^{\eta-}} \|\eta_s(t) - \eta(t)\| = \epsilon_\eta^* \\ \lim_{t\to t_{j+1}^{\alpha-}} \|\alpha_s(t) - \alpha(t)\| = \epsilon_\alpha^* \\ \lim_{t\to t_{m+1}^{\nu-}} \|\nu_s(t) - \nu(t)\| = \epsilon_\nu^* \\ \lim_{t\to t_{n+1}^{\tau-}} \|\tau_s(t) - \tau(t)\| = \epsilon_\tau^*. \end{cases} \tag{48}$$

As a result, it follows that:

$$\begin{cases} t_{i+1}^\eta - t_i^\eta \ge \varrho_\eta \\ t_{j+1}^\alpha - t_j^\alpha \ge \varrho_\alpha \\ t_{m+1}^\nu - t_m^\nu \ge \varrho_\nu \\ t_{n+1}^\tau - t_n^\tau \ge \varrho_\tau \end{cases} \tag{49}$$

where $\varrho_\eta = \epsilon_\eta^*/\hbar_\eta$, $\varrho_\alpha = \epsilon_\alpha^*/\hbar_\alpha$, $\varrho_\nu = \epsilon_\nu^*/\hbar_\nu$, and $\varrho_\tau = \epsilon_\tau^*/\hbar_\tau$. This means that there always exists a positive low upper bound of minimum interevent interval time during the period of communication and actuation. As a result, the Zeno phenomenon will not occur. ■

V. Experimental Results

In this section, experimental results are provided to illustrate the efficacy of the proposed event-triggered network-based path-tracking method for a USV. A small type of USV called CSICET-DH01 is designed with a motion control system, including micro control unit, a motion coprocessor, a global navigation satellite system receiver, an attitude sensor, and a ZigBee communication network. The entire experiment platform can be seen in Fig. 3. Experiments are conducted at the harbor basin of Dalian Maritime University at the Lingshui

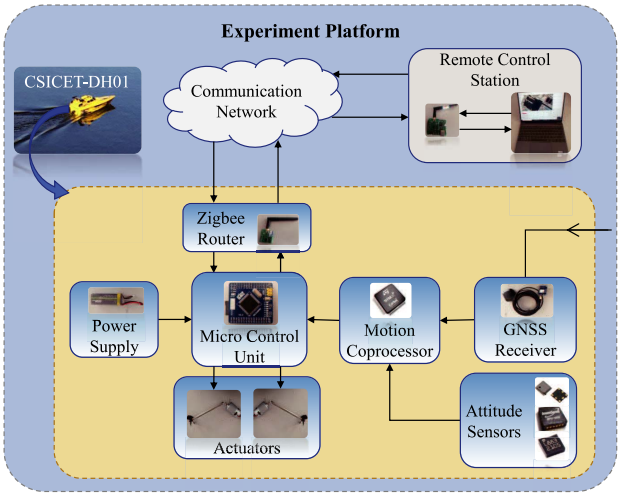

Fig. 3. Experiment platform of the CSICET-DH01 USV.

Port. In experiments, the USV is required to track a series of straight-line paths. The parametrized paths are set to

$$\begin{cases} p_{d1} = \mathrm{col}(21.6 - 0.4856\theta, 1302.5 + 0.8742\theta) \\ p_{d2} = \mathrm{col}(-22.1 - 0.8746(\theta - 90), 1381.2 \\ \qquad - 0.4848(\theta - 90)) \\ p_{d3} = \mathrm{col}(-100.8 + 0.4856(\theta - 180), 1337.63 \\ \qquad - 0.8742(\theta - 180)) \\ p_{d4} = \mathrm{col}(-61.7 + 0.8746(\theta - 260), 1267.7 \\ \qquad + 0.4848(\theta - 580)) \\ p_{d5} = \mathrm{col}(8.3 - 0.4856(\theta - 340), 1306.5 \\ \qquad + 0.8742(\theta - 340)) \\ p_{d6} = \mathrm{col}(-25.7 - 0.8746(\theta - 410), 1367.7 \\ \qquad - 0.4848(\theta - 410)) \\ p_{d7} = \mathrm{col}(-86.9 + 0.4856(\theta - 480), 1333.8 \\ \qquad - 0.8742(\theta - 480)) \\ p_{d8} = \mathrm{col}(-57.8 + 0.8746(\theta - 540), 1281.3 \\ \qquad + 0.4848(\theta - 540)) \\ p_{d9} = \mathrm{col}(-5.3 - 0.4856(\theta - 600), 1310.4 \\ \qquad + 0.8742(\theta - 600)) \\ p_{d10} = \mathrm{col}(-29.6 - 0.8746(\theta - 650), 1354.1 \\ \qquad - 0.4848(\theta - 650)) \\ p_{d11} = \mathrm{col}(-73 + 0.4856(\theta - 700), 1329.9 \\ \qquad - 0.8742(\theta - 700)) \\ p_{d12} = \mathrm{col}(-53.6 + 0.8746(\theta - 740), 1295 \\ \qquad + 0.4848(\theta - 740)) \\ p_{d13} = \mathrm{col}(-18.6 - 0.4856(\theta - 780), 1314.4 \\ \qquad + 0.8742(\theta - 780)) \\ p_{d14} = \mathrm{col}(33.2 - 0.8742(\theta - 800), 1340.5 \\ \qquad - 0.4848(\theta - 800)) \\ p_{d15} = \mathrm{col}(-59.4 + 0.4856(\theta - 830), 1325.8 \\ \qquad - 0.8742(\theta - 830)). \end{cases} \tag{50}$$

The kinematic guidance law (9) is implemented in the remote control center and the kinetic control law (21) is implemented in the micro control unit in the USV. The control parameters are selected as: $k_1 = 0.2$, $k_2 = 1$, $\Delta_1 = \Delta_3 = 1$, $\Delta_2 = 2$, $u_0 = 0.5$ m/s, $k_1^u = 1$, $k_2^u = 0.25$, $k_1^r = 0.1$, $k_2^r = 0.3$, $k_u = 2$, $k_r = -0.5$, $m_{11} = m_{33} = 1$, $\epsilon_\alpha^* = 0.4372$, $\epsilon_\tau^* = 0.1414$, $\epsilon_\nu^* = 0.03333$.

Fig. 4. Tracking performance of the CSICET-DH01 USV in the experiment.

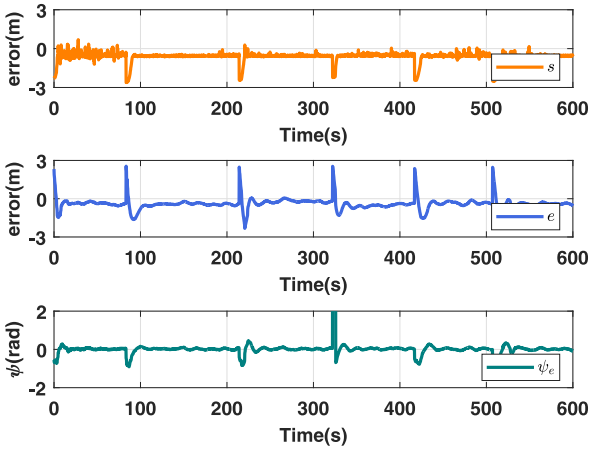

Fig. 5. Kinematic tracking errors in the experiment.

The experiments results are shown in Figs. 4–11. Fig. 4 depicts the trajectories of the USV and it can be seen that the USV is able to follow the path by using the proposed event-triggered network-based guidance law and control law with aperiodic communications and actuation. Fig. 5 plots the along-track, cross-track and yaw errors and it shows that they converge to a neighborhood of the origin. According to (4), the tracking errors suddenly increase when switching paths. As the positioning accuracy of the adopted GPS device is about 1.5 m, these tracking errors are acceptable in the sea environment. Fig. 6 shows the tracking performance of speed and yaw rate by the proposed event-triggered anti-disturbance control law. It can be observed that they are able to follow the commanded signals from the remote control law over wireless network. Fig. 7 plots the surge force τ_u and control moment τ_r, and they all bounded. The estimation performance of the ESOs are shown in Fig. 8. During transitions between different paths, the USV has to speed up and the total disturbance will increase. Note that the estimated disturbance of ESOs increase accordingly. This implies that the ESOs play their roles. Fig. 9 presents the event-triggered state of commanded speed and yaw rate from the remote control center. The event-triggered states of control inputs, actual total speed and yaw rate can be observed from Figs. 10 and 11. The triggering numbers in the steady phase are less than those in the transient phase. In Table I, the triggering times of α_U, α_r, τ_u, τ_r,

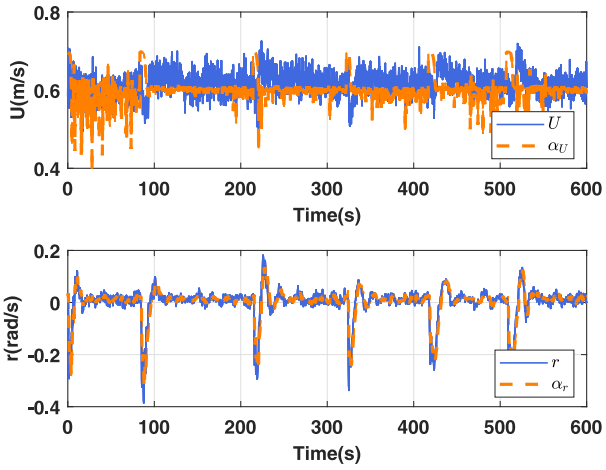

Fig. 6. Tracking performance of total speed and angular speed in the experiment.

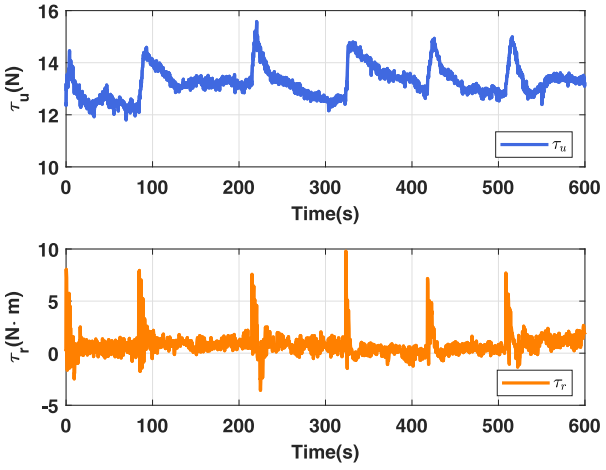

Fig. 7. Control inputs of the USV in the experiment.

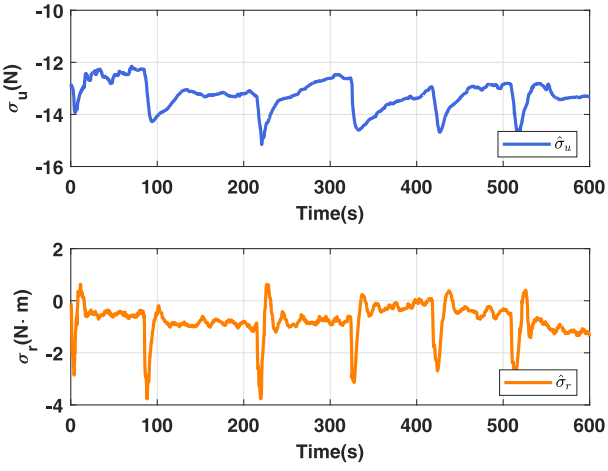

Fig. 8. ESO estimation of uncertainties in the experiment.

U, and r and their percentages with respect to periodic triggering times are listed. It is shown that the highest ratio is 21.7%, which implies that the proposed method can reduce the communication and actuation burden.

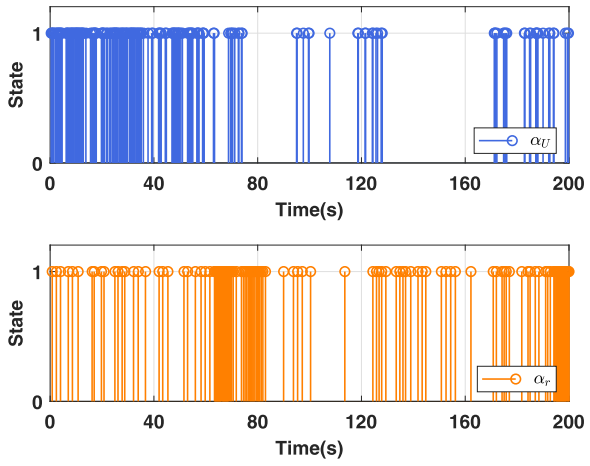

Fig. 9. Event-triggered state of desired commands in the experiment.

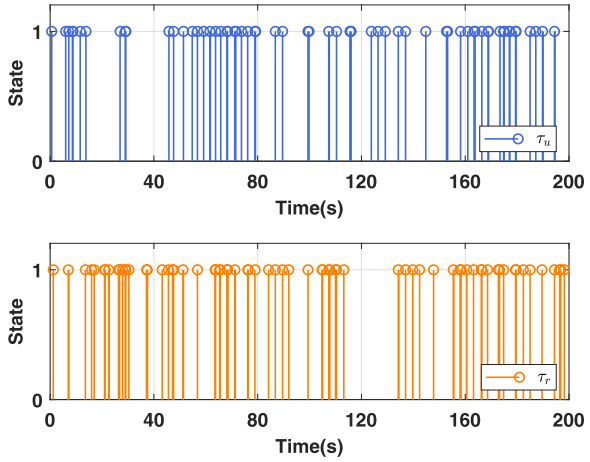

Fig. 10. Event-triggered state of control inputs in the experiment.

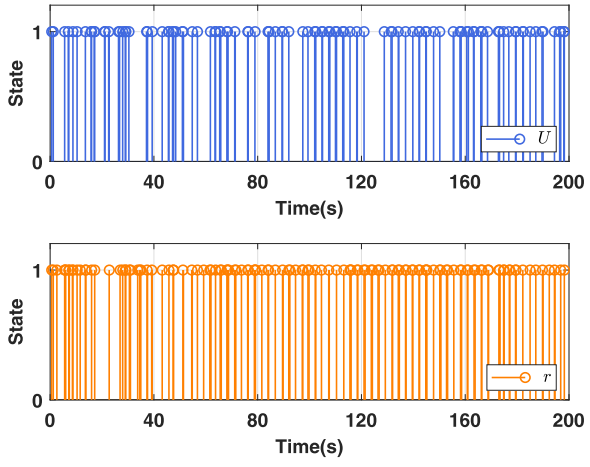

Fig. 11. Event-triggered state of actual total speed and angular speed in the experiment.

VI. Conclusion

A network-based path-tracking control method is proposed for a USV over the wireless network. The USV is subject to model uncertainties and unknown environmental disturbances, including wind, wave, and current, and a two-level network-based control architecture is presented, including a local inner loop and a remote outer loop. In the remote outer loop, an event-triggered guidance law based on the LOS principle is developed to track the predefined path and reduce the communication burden for the remote guidance side. The closed-loop guidance subsystem is proven to be ISS. In the local inner loop, two second-order ESOs are developed to estimate the uncertainties and unknown disturbances. An event-triggered control law based on the total estimated disturbances are presented for achieving the speed and angular speed tracking, which can also reduce actuation burden of the local inner loop. Then, the stability of the ESO subsystem and the kinetic subsystem are ISS by the input-to-state stability theory. The stability of the network-based closed-loop system is proved to be ISS by input-to-state and cascade stability theory. Finally, the proposed method is verified on an experiment platform of CSICET-DH01 USV. The experimental results demonstrated the effectiveness of the event-triggered network-based path-tracking control method.

TABLE I
Triggering Times and Their Percentages With Respect to the Periodic Communications or Actuations

Variables	Triggering Times	Percentage
α_U	217	21.7%
α_r	142	14.2%
τ_u	67	6.7%
τ_r	80	8.0%
U	120	12.0%
r	143	14.3%

Times of periodic communications or actuation: 1000

References

[1] Z. Liu, Y. Zhang, X. Yu, and C. Yuan, "Unmanned surface vehicles: An overview of developments and challenges," *Annu. Rev. Control*, vol. 41, pp. 71–93, 2016.

[2] Z. Peng, J. Wang, D. Wang, and Q.-L. Han, "An overview of recent advances in coordinated control of multiple autonomous surface vehicles," *IEEE Trans. Ind. Informat.*, vol. 17, no. 2, pp. 732–745, Feb. 2021.

[3] R. Cui, C. Yang, Y. Li, and S. Sharma, "Adaptive neural network control of AUVs with control input nonlinearities using reinforcement learning," *IEEE Trans. Syst., Man, Cybern., Syst.*, vol. 47, no. 6, pp. 1019–1029, Jun. 2017.

[4] W. He, Z. Yin, and C. Sun, "Adaptive neural network control of a marine vessel with constraints using the asymmetric barrier Lyapunov function," *IEEE Trans. Cybern.*, vol. 47, no. 7, pp. 1641–1651, Jul. 2017.

[5] R. Cui, S. S. Ge, B. V. E. How, and Y. S. Choo, "Leader–follower formation control of underactuated autonomous underwater vehicles," *Ocean Eng.*, vol. 37, nos. 17–18, pp. 1491–1502, Dec. 2010.

[6] S.-L. Dai, M. Wang, and C. Wang, "Neural learning control of marine surface vessels with guaranteed transient tracking performance," *IEEE Trans. Ind. Electron.*, vol. 63, no. 3, pp. 1717–1727, Mar. 2016.

[7] L. Liu, D. Wang, Z. Peng, C. L. P. Chen, and T. Li, "Bounded neural network control for target tracking of underactuated autonomous surface vehicles in the presence of uncertain target dynamics," *IEEE Trans. Neural Netw. Learn. Syst.*, vol. 30, no. 4, pp. 1241–1249, Apr. 2019.

[8] L. Liu, D. Wang, Z. Peng, and H. Wang, "Predictor-based LOS guidance law for path following of underactuated marine surface vehicles with sideslip compensation," *Ocean Eng.*, vol. 124, pp. 340–348, Sep. 2016.

[9] T. I. Fossen, K. Y. Pettersen, and R. Galeazzi, "Line-of-sight path following for dubins paths with adaptive sideslip compensation of drift forces," *IEEE Trans. Control Syst. Technol.*, vol. 23, no. 2, pp. 820–827, Mar. 2015.

[10] L. Liu, D. Wang, and Z. Peng, "ESO-based line-of-sight guidance law for path following of underactuated marine surface vehicles with

exact sideslip compensation," *IEEE J. Ocean. Eng.*, vol. 42, no. 2, pp. 477–487, Apr. 2017.

[11] Z. Peng, N. Gu, Y. Zhang, Y. Liu, D. Wang, and L. Liu, "Path-guided time-varying formation control with collision avoidance and connectivity preservation of under-actuated autonomous surface vehicles subject to unknown input gains," *Ocean Eng.*, vol. 191, Nov. 2019, Art. no. 106501.

[12] Y.-Y. Chen and Y.-P. Tian, "A curve extension design for coordinated path following control of unicycles along given convex loops," *Int. J. Control*, vol. 84, no. 10, pp. 1729–1745, Oct. 2011.

[13] Z. Peng, Y. Jiang, and J. Wang, "Event-triggered dynamic surface control of an underactuated autonomous surface vehicle for target enclosing," *IEEE Trans. Ind. Electron.*, vol. 68, no. 4, pp. 3402–3412, Apr. 2021.

[14] Y. Jiang, Z. Peng, D. Wang, and C. L. P. Chen, "Line-of-sight target enclosing of an underactuated autonomous surface vehicle with experiment results," *IEEE Trans. Ind. Informat.*, vol. 16, no. 2, pp. 832–841, Feb. 2020.

[15] L. Zhang, H. Gao, and O. Kaynak, "Network-induced constraints in networked control systems—A survey," *IEEE Trans. Ind. Informat.*, vol. 9, no. 1, pp. 403–416, Feb. 2013.

[16] Q. Zhang, L. Lapierre, and X. Xiang, "Distributed control of coordinated path tracking for networked nonholonomic mobile vehicles," *IEEE Trans. Ind. Informat.*, vol. 9, no. 1, pp. 472–484, Feb. 2013.

[17] K. D. Do, "Synchronization motion tracking control of multiple underactuated ships with collision avoidance," *IEEE Trans. Ind. Electron.*, vol. 63, no. 5, pp. 2976–2989, May 2016.

[18] N. Gu, Z. Peng, D. Wang, Y. Shi, and T. Wang, "Antidisturbance coordinated path following control of robotic autonomous surface vehicles: Theory and experiment," *IEEE/ASME Trans. Mechatron.*, vol. 24, no. 5, pp. 2386–2396, Oct. 2019.

[19] W. Caharija *et al.*, "Integral line-of-sight guidance and control of underactuated marine vehicles: Theory, simulations, and experiments," *IEEE Trans. Control Syst. Technol.*, vol. 24, no. 5, pp. 1623–1642, Sep. 2016.

[20] A. M. Lekkas and T. I. Fossen, "Integral LOS path following for curved paths based on a monotone cubic hermite spline parametrization," *IEEE Trans. Control Syst. Technol.*, vol. 22, no. 6, pp. 2287–2301, Nov. 2014.

[21] Z. Peng, J. Wang, and D. Wang, "Distributed maneuvering of autonomous surface vehicles based on neurodynamic optimization and fuzzy approximation," *IEEE Trans. Control Syst. Technol.*, vol. 26, no. 3, pp. 1083–1090, May 2018.

[22] R. Skjetne, T. I. Fossen, and P. V. Kokotović, "Adaptive maneuvering, with experiments, for a model ship in a marine control laboratory," *Automatica*, vol. 41, no. 2, pp. 289–298, Feb. 2005.

[23] L. Liu, D. Wang, Z. Peng, and T. Li, "Modular adaptive control for LOS-based cooperative path maneuvering of multiple underactuated autonomous surface vehicles," *IEEE Trans. Syst., Man, Cybern., Syst.*, vol. 47, no. 7, pp. 1613–1624, Jul. 2017.

[24] Z. Peng, J. Wang, and D. Wang, "Distributed containment maneuvering of multiple marine vessels via neurodynamics-based output feedback," *IEEE Trans. Ind. Electron.*, vol. 64, no. 5, pp. 3831–3839, May 2017.

[25] Z. Peng, J. Wang, and D. Wang, "Containment maneuvering of marine surface vehicles with multiple parameterized paths via spatial-temporal decoupling," *IEEE/ASME Trans. Mechatron.*, vol. 22, no. 2, pp. 1026–1036, Apr. 2017.

[26] Y.-L. Wang, Q.-L. Han, M.-R. Fei, and C. Peng, "Network-based T-S fuzzy dynamic positioning controller design for unmanned marine vehicles," *IEEE Trans. Cybern.*, vol. 48, no. 9, pp. 2750–2763, Sep. 2018.

[27] R. Cui, X. Zhang, and D. Cui, "Adaptive sliding-mode attitude control for autonomous underwater vehicles with input nonlinearities," *Ocean Eng.*, vol. 123, pp. 45–54, Sep. 2016.

[28] Z. Peng, J. Wang, and J. Wang, "Constrained control of autonomous underwater vehicles based on command optimization and disturbance estimation," *IEEE Trans. Ind. Electron.*, vol. 66, no. 5, pp. 3627–3635, May 2019.

[29] J. Gao, A. A. Proctor, Y. Shi, and C. Bradley, "Hierarchical model predictive image-based visual servoing of underwater vehicles with adaptive neural network dynamic control," *IEEE Trans. Cybern.*, vol. 46, no. 10, pp. 2323–2334, Oct. 2016.

[30] Z. Peng and J. Wang, "Output-feedback path-following control of autonomous underwater vehicles based on an extended state observer and projection neural networks," *IEEE Trans. Syst., Man, Cybern., Syst.*, vol. 48, no. 4, pp. 535–544, Apr. 2018.

[31] L. Liu, D. Wang, and Z. Peng, "State recovery and disturbance estimation of unmanned surface vehicles based on nonlinear extended state observers," *Ocean Eng.*, vol. 171, pp. 625–632, Jan. 2019.

[32] Z. Peng, D. Wang, T. Li, and M. Han, "Output-feedback cooperative formation maneuvering of autonomous surface vehicles with connectivity preservation and collision avoidance," *IEEE Trans. Cybern.*, vol. 50, no. 6, pp. 2527–2535, Jun. 2020.

[33] X.-M. Zhang *et al.,* "Networked control systems: A survey of trends and techniques," *IEEE/CAA J. Autom. Sinica*, vol. 7, no. 1, pp. 1–17, Jan. 2020.

[34] Y.-L. Wang and Q.-L. Han, "Network-based modelling and dynamic output feedback control for unmanned marine vehicles in network environments," *Automatica*, vol. 91, pp. 43–53, May 2018.

[35] Y.-L. Wang and Q.-L. Han, "Network-based fault detection filter and controller coordinated design for unmanned surface vehicles in network environments," *IEEE Trans. Ind. Informat.*, vol. 12, no. 5, pp. 1753–1765, Oct. 2016.

[36] Y.-L. Wang and Q.-L. Han, "Network-based heading control and rudder oscillation reduction for unmanned surface vehicles," *IEEE Trans. Control Syst. Technol.*, vol. 25, no. 5, pp. 1609–1620, Sep. 2017.

[37] I.-A. F. Ihle, M. Arcak, and T. I. Fossen, "Passivity-based designs for synchronized path-following," *Automatica*, vol. 43, no. 9, pp. 1508–1518, Sep. 2007.

[38] Y. Zhang, D. Wang, Z. Peng, T. Li, and L. Liu, "Event-triggered ISS-modular neural network control for containment maneuvering of nonlinear strict-feedback multi-agent systems," *Neurocomputing*, vol. 377, pp. 314–324, Feb. 2020.

[39] Y.-Y. Chen and Y.-P. Tian, "Coordinated path following control of multi-unicycle formation motion around closed curves in a time-invariant flow," *Nonlinear Dyn.*, vol. 81, nos. 1–2, pp. 1005–1016, Apr. 2015.

[40] Z. Zheng and M. Feroskhan, "Path following of a surface vessel with prescribed performance in the presence of input saturation and external disturbances," *IEEE/ASME Trans. Mechatron.*, vol. 22, no. 6, pp. 2564–2575, Dec. 2017.

[41] Z. Peng, J. Wang, and Q.-L. Han, "Path-following control of autonomous underwater vehicles subject to velocity and input constraints via neurodynamic optimization," *IEEE Trans. Ind. Electron.*, vol. 66, no. 11, pp. 8724–8732, Nov. 2019.

[42] S.-R. Oh and J. Sun, "Path following of underactuated marine surface vessels using line-of-sight based model predictive control," *Ocean Eng.*, vol. 37, pp. 289–295, Feb. 2010.

[43] T. I. Fossen and K. Y. Pettersen, "On uniform semiglobal exponential stability (USGES) of proportional line-of-sight guidance laws," *Automatica*, vol. 50, no. 11, pp. 2912–2917, Nov. 2014.

[44] M. Lv, D. Wang, Z. Peng, L. Liu, and H. Wang, "Event-triggered neural network control of autonomous surface vehicles over wireless network," *Inf. Sci.*, vol. 63, May 2020, Art. no. 150205.

[45] L. Liu, D. Wang, Z. Peng, T. Li, and C. L. P. Chen, "Cooperative path following ring-networked under-actuated autonomous surface vehicles: Algorithms and experimental results," *IEEE Trans. Cybern.*, vol. 50, no. 4, pp. 1519–1529, Apr. 2020.

[46] T. I. Fossen, *Handbook of Marine Craft Hydrodynamics and Motion Control*. Chichester, U.K.: Wiley, 2011.

[47] H. K. Khalil, *Nonlinear Control*. Harlow, U.K.: Pearson Educ., 2015.

Wentao Wu received the B.E. degree in electrical engineering and automation from the Harbin University of Science and Technology, Harbin, China, in 2018. He is currently pursuing the M.E. degree in electrical engineering with Dalian Maritime University, Dalian, China.

He conducted academic exchanges in the Science and Technology on Underwater Vehicle Technology, Harbin Engineering University, Harbin, in 2020. His current research interest is guidance and control of unmanned surface vehicles.

Zhouhua Peng (Senior Member, IEEE) received the B.E. degree in electrical engineering and automation, the M.E. degree in power electronics and power drives, and the Ph.D. degree in control theory and control engineering from Dalian Maritime University, Dalian, China, in 2005, 2008, and 2011, respectively.

In 2011, he joined the School of Marine Engineering, Dalian Maritime University, where he is currently a Professor with the School of Marine Electrical Engineering. From 2014 to 2018, he was a Postdoctoral Research Fellow with the School of Control Science and Engineering, Dalian University of Technology, Dalian. From 2016 to 2018, he was a Hong Kong Scholar with the Department of Computer Science, City University of Hong Kong, Hong Kong, where he was a Senior Research Fellow with the Department of Computer Science, in 2019. He has authored over 190 refereed publications. His research interest is cooperative control of multiple autonomous surface vehicles.

Prof. Peng was a recipient of the Science and Technology Award (First Class) from China Association of Oceanic Engineering in 2019, the Natural Science Awards (Second Class) from Liaoning Province in 2013 and 2017, the Hong Kong Scholar Award in 2016, and the Science and Technology Award for Youth from China Institute of Navigation in 2017. He won the Honor of the Distinguished Worker in the National Ministry of Transport of China in 2020, the Science and Innovation Leadership for Young and Middle-aged Scientists of the Ministry of Transport of the People's Republic of China in 2020, the "Bai-Qian-Wan" Talent (level Bai) from Liaoning Province in 2019, the Young Talent in Science and Technology from the Ministry of Transport of the People's Republic of China in 2017, and the Distinguished Young Talent in Science and Technology from Dalian in 2018.

Dan Wang (Senior Member, IEEE) received the B.E. degree in industrial automation engineering from the Dalian University of Technology, Dalian, China, in 1982, the M.E. degree in marine automation engineering from Dalian Maritime University, Dalian, in 1987, and the Ph.D. degree in mechanical and automation engineering from The Chinese University of Hong Kong, Hong Kong, in 2001.

He is a Professor with the School of Marine Electrical Engineering, Dalian Maritime University. From 2001 to 2005, he was a Research Scientist with Temasek Laboratories, National University of Singapore, Singapore. In 2012, he was a Visiting Professor with the Institute for Aerospace Studies, University of Toronto, Toronto, ON, Canada. He has authored over 220 refereed publications. His research interests include nonlinear control theory and its applications.

Lu Liu (Member, IEEE) received the B.E. degree in electrical engineering and automation and the Ph.D. degree in marine electrical engineering from Dalian Maritime University, Dalian, China, in 2012 and 2018, respectively.

In 2018, she joined the School of Marine Engineering, Dalian Maritime University, where she is currently an Associate Professor with the School of Marine Electrical Engineering and a Postdoctoral Research Fellow with the School of Electrical Information and Electric Engineering, Shanghai Jiaotong University, Shanghai, China. She has authored over 40 refereed publications. Her research interests include guidance and control of single/multiple marine surface vehicles.

Qing-Long Han (Fellow, IEEE) received the B.Sc. degree in mathematics from Shandong Normal University, Jinan, China, in 1983, and the M.Sc. and Ph.D. degrees in control engineering from the East China University of Science and Technology, Shanghai, China, in 1992 and 1997, respectively.

He is a Pro Vice-Chancellor (Research Quality) and a Distinguished Professor with Swinburne University of Technology, Melbourne, VIC, Australia. He held various academic and management positions with Griffith University, Gold Coast, QLD, Australia, and Central Queensland University, Rockhampton, QLD. His research interests include networked control systems, multi-agent systems, time-delay systems, smart grids, unmanned surface vehicles, and neural networks.

Dr. Han was the recipient of the 2021 M. A. Sargent Medal (the Highest Award of the Electrical College Board of Engineers Australia), the 2020 IEEE Systems, Man, and Cybernetics (SMC) Society Andrew P. Sage Best Transactions Paper Award, the 2020 IEEE Transactions on Industrial Informatics Outstanding Paper Award, and the 2019 IEEE SMC Society Andrew P. Sage Best Transactions Paper Award. He was a Highly Cited Researcher in Engineering and Computer Science (Clarivate Analytics, 2019–2020). He is a Co-Editor of *Australian Journal of Electrical and Electronic Engineering*, an Associate Editor for 12 international journals, including the IEEE TRANSACTIONS ON CYBERNETICS, the IEEE TRANSACTIONS ON INDUSTRIAL INFORMATICS, *IEEE Industrial Electronics Magazine*, the IEEE/CAA JOURNAL OF AUTOMATICA SINICA, *Control Engineering Practice*, and *Information Sciences*, and a guest editor for 13 special issues. He has served as an AdCom Member of IEEE Industrial Electronics Society (IES), a Member of IEEE IES Fellow Committee, and the Chair of IEEE IES Technical Committee on Networked Control Systems. He was one of Australia's Top Five Lifetime Achievers (Research Superstars) in Engineering and Computer Science (The Australian's 2020 Research Magazine). He is a Fellow of The Institution of Engineers Australia.